Bulletin of Volcanology (2020) 82: 35
https://doi.org/10.1007/s00445-020-01374-8

RESEARCH ARTICLE

Towards a satellite-based approach to measure eruptive volumes at Mt. Etna using Pleiades datasets

Cristina Proietti[1] · Mauro Coltelli[1] · Maria Marsella[2] · Michele Martino[2,3] · Silvia Scifoni[2,3] · Francesca Giannone[4]

Received: 17 April 2019 / Accepted: 16 March 2020 / Published online: 30 March 2020

Abstract

Only a few high precision studies of lava and tephra during simultaneous explosive and effusive activity have so far been undertaken. We carried out such measurements by analysis of a unique and homogeneous multi-temporal dataset of high-spatial resolution satellite optical images. Digital Elevation Models (DEMs) and orthophotos (with 1- and 0.5-m-pixel resolutions respectively) were extracted from six specifically tasked Pleiades tri-stereo pairs of Mt. Etna volcano, between 2011 and 2016. During this period, frequent effusive and explosive events formed lava flow fields and built up the new south-east crater pyroclastic cone. The volumes of lava fields and proximal pyroclastic deposits were measured by comparing the Pleiades DEMs with an aerial photogrammetric DEM updated in 2007. The volumes of all distal deposits were estimated using lava and tephra partitioning from the literature for an Etnean lava fountain. The dense rock equivalent volume of lava and tephra, calculated to be $248.4 \pm 2.1 \times 10^6$ m^3 in total, corresponds to an average output rate of 0.98 m^3/s over the analysed 8-year period (May 2008–May 2016) and to a multi-event eruption rate of 5.53 m^3/s for 520 days of activity. The multi-temporal analysis of high-spatial resolution satellite DEMs, here successfully applied to the well-monitored Etna volcano, demonstrated that the tasking of high-spatial resolution satellite images is crucial for fast and effective monitoring during intense volcanic activity (frequent and overlapping eruptive events). This methodology could be used for the monitoring of remote or hazardous volcanoes that are difficult to study by means of repeated field surveys.

Editorial responsibility: M.R. James

✉ Cristina Proietti
cristina.proietti@ingv.it

Mauro Coltelli
mauro.coltelli@ingv.it

Maria Marsella
maria.marsella@uniroma1.it

Michele Martino
michele.martino@serco.it

Silvia Scifoni
Silvia.Scifoni@serco.com

Francesca Giannone
francesca.giannone@unicusano.it

[1] Istituto Nazionale di Geofisica e Vulcanologia Osservatorio Etneo, Piazza Roma 2, 95125 Catania, Italy

[2] Dipartimento di Ingegneria Civile, Edile e Ambientale (D.I.C.E.A), Università di Roma La Sapienza, Via Eudossiana 18, 00184 Rome, Italy

[3] Serco Italia S.p.A., Via Sciadonna 24-26, 00044 Frascati, Rome, Italy

[4] Università Niccolò Cusano, Via Don Carlo Gnocchi 3, 00166 Rome, Italy

Keywords Pleiades satellite · High-spatial resolution DEM · Etna volcano · Eruption volume · Magma output rate

Introduction

Rapid and frequent morphological changes on active volcanoes can make it necessary to update topographic data, such as DEMS and orthophotos, over large areas both during and after eruptions to support risk assessment and mitigation actions. Airborne or satellite remote sensing techniques offering three-dimensional (3-D) mapping capability are preferable to ground-based topographic instruments in order to acquire data covering wider areas from a safe distance, and as frequently and accurately as possible. Satellite observations have an increasingly important role in advancing the understanding of the volcanic behaviour and are especially useful on remote volcanoes where field or airborne surveys are challenging (e.g. Mouginis-Mark et al. 1989; Francis and Rothery 2000; Rowland et al. 2003; Bagnardi et al. 2016; Martino et al. 2016; Bonny et al. 2018).

Ground-based measurements enable the volume of morphological change, in particular of lava flows, to be quantified through a planimetric approach in which the planimetric area

of change is multiplied by an average thickness (Stevens et al. 1999). Global Positioning System (GPS) surveys or close-range orthorectified digital images can be used to measure the area, while thickness can be measured using total stations or GPS and laser rangefinder (e.g. Calvari et al. 1994; Honda and Nagai 2002; Behncke et al. 2014; Marsella et al. 2014; Naranjo et al. 2016; Coltelli et al. 2017; Bonny et al. 2018). Lava thicknesses are mostly measured on flow margins and fronts and might not be representative of central thickness due to surface roughness. This discrepancy is even more relevant for long-duration complex lava fields emplaced on irregular topographies. In these cases, the lava morphology is poorly represented by the limited number of measurements and by a simplified segmentation of the flow fields based on the slope of the pre-existing topography; thus, the planimetric volume estimation can have an error greater than 20% (Calvari et al. 1994).

Aerial and satellite remote sensing techniques enable the area, volume and thickness of morphological change to be quantified through a topographic approach based on the comparison of DEMs acquired before, during and after an eruption (Stevens et al. 1999). Digital photogrammetry is one of the most flexible tools for producing high-spatial resolution (Ground Sampling Distance, GSD, from millimetres to meters depending on the viewing distance) DEMs and orthophotos of rough terrain, such as volcanoes, and can provide sub-meter accuracy (Marsella et al. 2009; Dvigalo et al. 2016). However, aerial photogrammetry can be limited by the hazard posed by an active volcano and by the costs and duration (from hours to days) of image acquisition that increase with the total area to be covered and with the requested spatial resolution (a smaller GSD implies a lower flight height, resulting in smaller area on each image and longer acquisition times). These limits are overcome by space-borne Earth Observation (EO) optical sensors acquiring stereo and tri-stereo scenes with meter (Ikonos and Quickbird) to sub-meter (WorldView and Pleiades) GSD, enabling DEMs and orthophotos to be derived at relatively high temporal frequency (hours to days, if using multiple platforms) and meter-level accuracy. In comparison with aerial data, satellite data provide wider coverage from a single pass thanks to a larger swath width, for example 16.4 km and 20 km at nadir for WorldView and Pleiades, respectively. Other satellite sensors acquire datasets with moderate-to-high spatial resolution (~ 10 to 100 m GSD such as ASTER, SRTM and SPOT) and generally low temporal frequency (revisiting time of 16, 26 and 1–5 days for ASTER, SPOT 4, 5 and SPOT 7, respectively).

To explore the possibilities of volcano monitoring through specifically tasked acquisitions, from meter-resolution satellite systems, we carried out photogrammetric processing of optical images, most of which were acquired by the Pleiades spacecraft. The twin spacecraft Pleiades-1A and Pleiades-1B, in operation since December 2011 and December 2012, are capable of daily revisits to any point on the globe and of acquiring panchromatic and multi-spectral images with GSD of 0.5 m and 2 m, respectively (Boissin et al. 2012). Image acquisition can be tasked for specific areas and this is especially valuable for volcano monitoring during eruption crises. From a single pass, Pleiades satellites can capture stereoscopic near-nadir looks in addition to classic forward and backward looks (tri-stereo) allowing a better retrieval of height data over terrains with high roughness, steep slopes and shadows. Pleiades high-spatial resolution DEMs were used for quantifying the 2014–2015 lava field of Fogo Volcano, Cape Verde, showing better performance on lava flow surfaces than on ash and cinder (Bagnardi et al. 2016). A 2015 Pleiades DEM was compared with a photogrammetric DEM of 2005 for quantifying the volume of all 2005–2015 eruptive products and of the new South-East crater cone (Ganci et al. 2018).

In this study, we exploited high-spatial resolution optical images of the Pleiades satellites, acquired after a specific data tasking in the framework of a scientific collaboration within the Space Volcano Observatory with Pleiades (SVOP) project (http://volcano.iterre.fr/svo_projects). This project was aimed at acquiring data for monitoring the morphological changes in hazardous and/or unreachable areas, such as active volcanoes, and for producing results useful to hazard assessment. Mount Etna was selected as the study area because frequent effusive and explosive eruptive events have recently modified its summit morphology, emplacing compound lava fields and building up the New South-East Crater (NSEC) pyroclastic cone. The analysis of a time-series of DEMs and orthophotos, extracted from Pleiades images, allowed us measuring the volumes of effusive and explosive (proximal) products erupted at Etna between 2008 and 2016, while quantifying the associated precisions. The distal products were estimated by applying the relationship between the dense rock equivalent volumes of effusive and explosive products that were precisely measured, for the first time, for the 25–26 October 2013 lava fountain on Etna (Andronico et al. 2018). In this way, we measured, through a unique methodology, the total volume (effusive and explosive) of magma erupted at Etna, over an 8-year period, and the output rate, which are key data for understanding eruptive behaviours and assessing relative hazards. Quantifying the volume of the different products of a frequently active volcano can be very difficult; previously published work analysing Etna's recent eruptive activity generally evaluated the total volumes by combining measurements obtained with different techniques.

The acquisition of optical images of Etna from Pleiades satellites enabled monitoring of the intense volcanic activity, which was characterized by frequent events and overlapping eruptive products. The tri-stereo acquisition, the large swath width and the high-spatial resolution of Pleiades images enabled us to directly extract, from a single pass, DEMs and orthophotos (with meter and sub-meter GSD, respectively) of the whole area covered by the eruptive activity and to adequately map different eruptive products. During intense volcanic activity, image tasking is crucial in order to effectively

survey the volcano and quantify the related hazard because it makes it possible to distinguish eruptive events separated by a few days. The capacity to directly georeference satellite material reduces or eliminates the need to perform field surveys to measure Ground Control Points (GCPs), although they can help improve the georeferencing. Therefore, the acquisition and analysis of tasked satellite optical images is a methodology highly suited to the monitoring of volcanic eruptions, and it is also faster and safer than surveys based on field or aerial data.

The 2007–2016 eruptive activity of Mt. Etna

Since 2007, Etna eruptive activity has mainly occurred in its summit area (Fig. 1), particularly in the New South-East Crater (NSEC), while the other craters Bocca Nuova, North East Crater, South-East Crater and Voragine (BN, NEC, SEC and VOR) have been only occasionally active (Fig. 2). Powerful lava fountains occurred at SEC on 4–5 September 2007, 23–24 November 2007 and 10 May 2008, forming ash plumes and lava flows that extended over the upper Valle del Bove (VdB). Between 13 May 2008 and 6 July 2009, a lateral effusive eruption from vents close to the summit area produced a compound lava field on VdB that covered the 2007–2008 flows (Behncke et al. 2016). Subsequently, after a period of only minor activity, an intense and frequent succession of discrete explosive and effusive events (Fig. 2) substantially modified Etna's summit morphology between 2011 and 2016. Compound lava flow fields formed on the East, South and West flanks and the NSEC pyroclastic cone rapidly

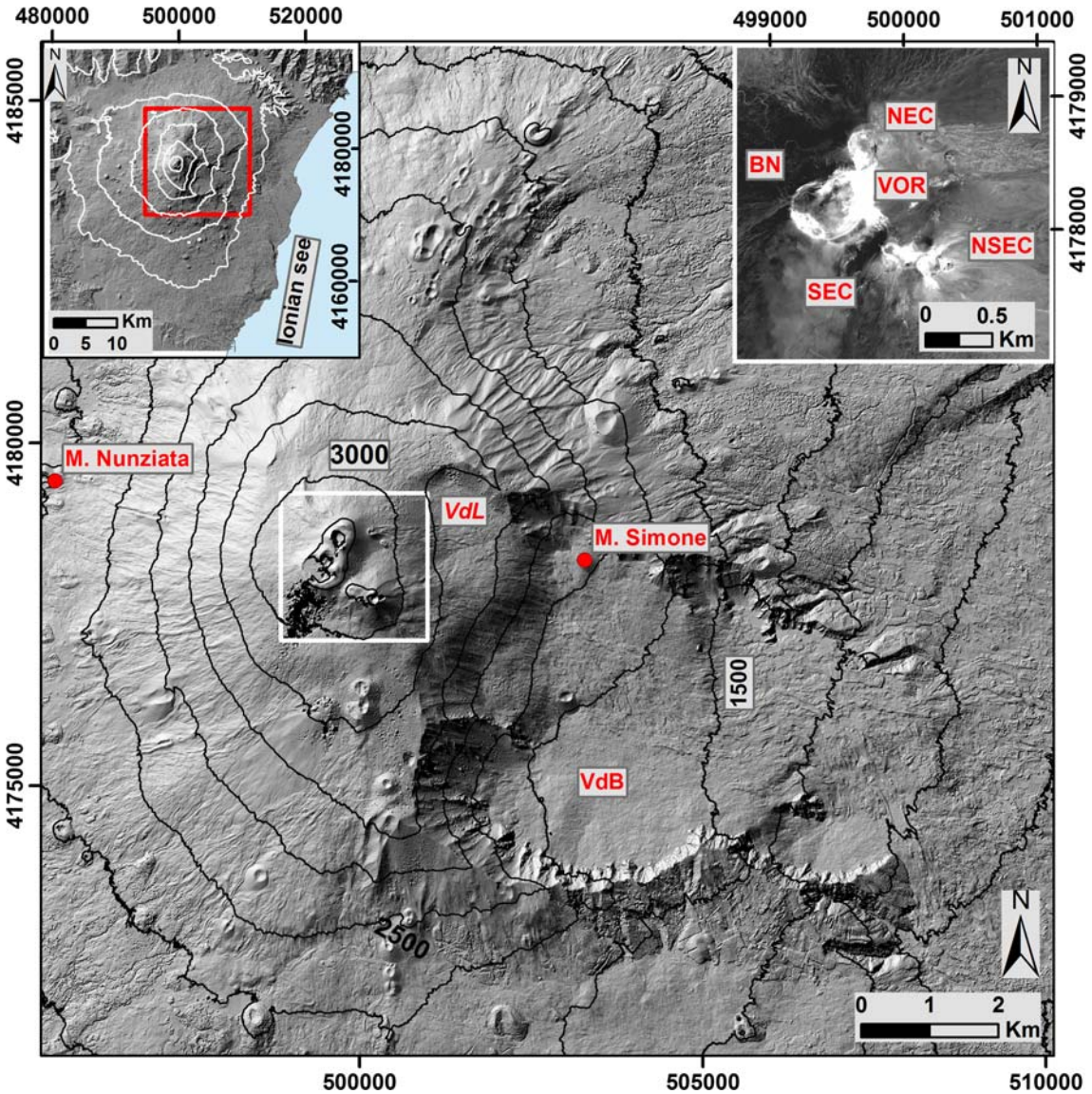

Fig. 1 Shaded relief of the 18 July 2016 Pleiades DEM with contour lines of height above the geoid every 250 m. Right inset shows Etna summit area (white square) from the 18 July 2016 orthophoto. Left inset locates the investigated area (red square) on the 2005 Etna shaded relief (Gwinner et al. 2006) with contour lines of geoid height every 500 m

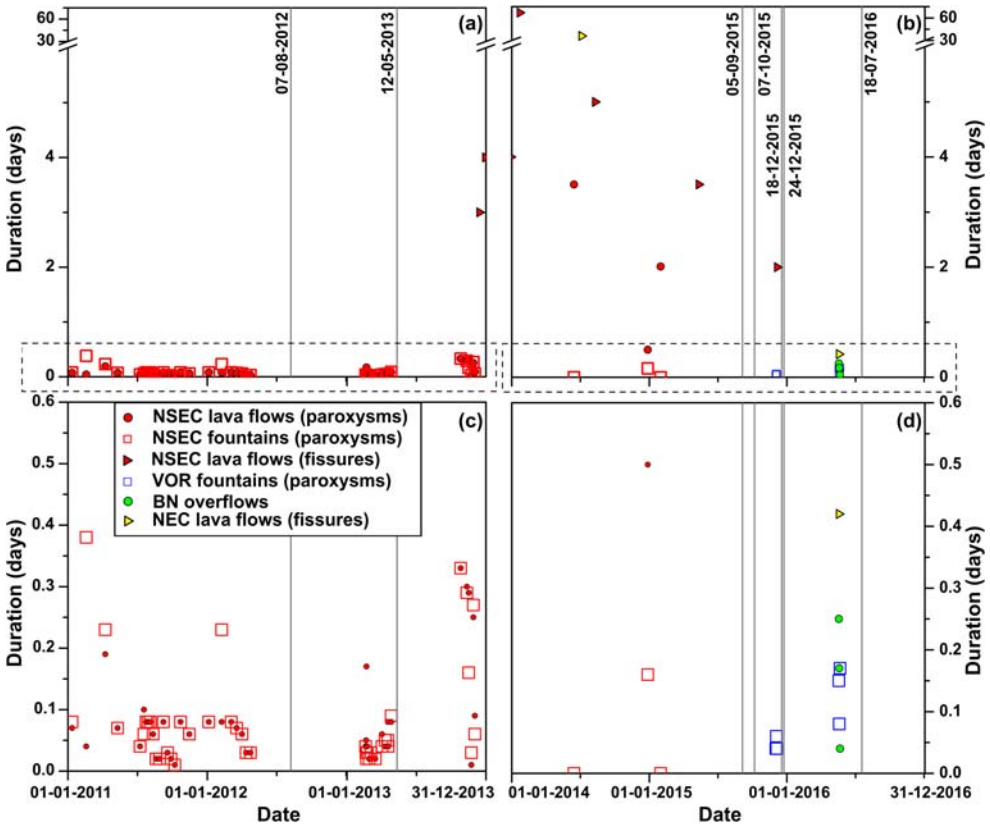

Fig. 2 Duration of the different eruptive events from 2011 to 2013 (**a**) and from 2014 to 2016 (**b**). **c**, **d** Enlargements of the dashed rectangles in (**a**) and (**b**). Grey vertical lines indicate the timing of DEM acquisitions

grew on the east flank of SEC (Behncke et al. 2014; De Beni et al. 2015; Corsaro et al. 2017).

Forty-five eruptive events characterized by brief but powerful strombolian, lava fountain and effusive phases, named paroxysms, caused the growth of the NSEC cone (up to a height of about 200 m) and formed compound lava flow fields in VdB (partially covering the 2008–2009 one) and on the south flank. Lava fountains lasted between 30 min and 9 h while concurrent flows were active for up to 12 h. Frequent eruptive events alternated with pauses of several months. Twenty-five, thirteen and six paroxysms occurred from January 2011–April 2012, February–April 2013 and October–December 2013, respectively. Subsequently, only five strombolian and effusive events, lasting from 2 to 67 days, occurred from vents on NSEC flanks and rims up to August 2014. The last paroxysm occurred on 28–29 December 2014. Strong strombolian and effusive activity occurred from 31 January to 2 February 2015; a fissure on the NSEC north-eastern flank, just below the crater rim, was active from 12 to 16 May 2015 and three effusive vents on the NSEC high east flank fed single flows from 6 to 8 December 2015.

The VOR, which last erupted in 1999, underwent intense explosive activity from 27 February 2013 that lasted, with decreasing intensity, until 17 March. Strombolian activity resumed in late October 2015 and increased on 2 December. Four paroxysmal lava fountains occurred from 3 to 5 December 2015, forming ash plumes up to 14 km high and proximal deposits that filled the crater and overflowed into the adjoining BN. A new sequence of paroxysmal events occurred from 18 to 25 May 2016, including three lava fountains and intense strombolian activity, the products of which overflowed into the adjoining BN, as well as a small lava flow from a fissure in the saddle between VOR and SEC.

The BN, which last erupted in 2002, showed strombolian activity on 11 July 2011 and within a few days formed a lava flow that covered its crater floor. Between July and October 2012, short strombolian episodes built a small cone and new lava flowed onto the crater floor. Vigorous strombolian activity periodically occurred in January–February 2013. Then on 18, 19 and 21 May 2016, the lava erupted from VOR paroxysms overflowed into BN and went on to overflow from its lower western rim, producing three overlapping lava fields on the western flank, towards M. Nunziata, that stopped at 1800 m a.s.l.

Small and periodic ash emissions and thermal anomalies have been observed at NEC since 15 December 2013. Fissures on NEC eastern flank, from 5 July to 10 August 2014, produced strong strombolian activity and lava flows from Valle del Leone (VdL) to the upper VdB, and a lava flow into VdB towards M. Simone on 18–19 May 2016.

Data and methods

A multi-temporal dataset of optical satellite images comprising two stereo-couples acquired in 2012 and 2013 from

Worldview-2 and Pleiades satellites, respectively, as well as five Pleiades tri-stereo acquisitions between 2015 and 2016 (Table 1), was collected. Pleiades datasets were processed with the OrthoEngine tool implemented in PCI Geomatics software (www.pcigeomatics.com), to extract geocoded DEMs and orthophotos (UTM planimetric datum and ellipsoid, WGS-84, elevations). Image corrections were applied using the rational polynomial functions model based on the Rational Polynomial Coefficients (RPCs), delivered as image metadata, that provide a compact representation of a ground-to-image geometry without the need to measure 3-D GCPs (Fraser et al. 2006). However, to increase the accuracy of DEM georeferencing, the initial RCP functions can be refined by using GCPs measured on the ground or on reference maps. Here, we measured the coordinates of 45 GCPs on Etna's orthophotos (GSDs of 0.25 m) and DEMs (1 × 1 m grid) obtained in 2005 with the airborne High-spatial Resolution Stereo Camera (HRSC-AX) sensor and photogrammetric processing system (Gwinner et al. 2006). Automatic DEM extraction from the Pleiades datasets was based on the Semi-Global Matching method which is particularly efficient in low contrast areas (Eisank et al. 2015). The use of the same GCPs for all Pleiades datasets guarantees co-registration between the various DEMs and therefore the repeatability of measurements from multi-temporal comparisons. An overall accuracy of greater than 0.6 m (Fig. 3) was obtained for both the horizontal and vertical components by analysing the discrepancy between the coordinates of 11 additional Check Points (CPs) measured on the 2005 datasets and on the Pleiades models. Therefore, the final GSD for Pleiades DEMs and orthophotos was set to 1 m and 0.5 m, respectively. Automatic processing of the 2012 Worldview-2 stereo-couple failed owing to the presence of clouds and a volcanic plume, so the data were processed through a manual photogrammetric restitution with the Helava software (Baldi et al. 2005), to extract the DEM of the NSEC area. A DEM acquired in August 2007 (10 × 10 m grid, UTM planimetric datum and geoid elevations), with the airborne High-spatial Resolution Stereo Camera (HRSC-AX) sensor and photogrammetric processing system (Gwinner et al. 2006) to update the topography of Etna's summit area, was also analysed because it represents the topographic surface before the 2007–2016 eruptive activity.

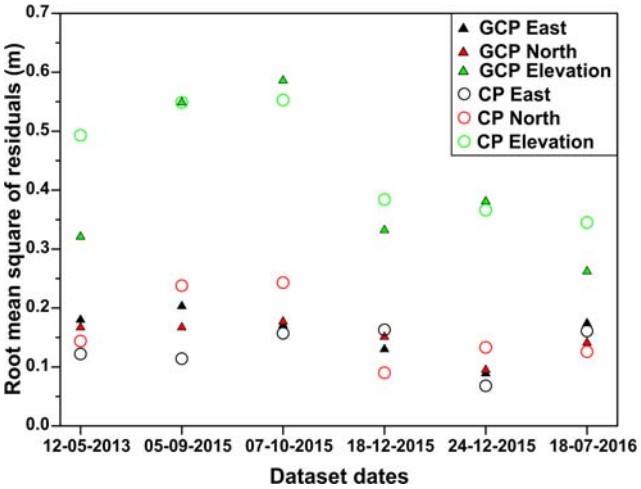

Fig. 3 Root mean square of the discrepancies between the coordinates, measured on the Pleiades and the 2005 DEMs, for GCPs and CPs (full triangles and empty circles, respectively)

The topographic approach was applied to the multi-temporal dataset to quantify the bulk volumes of lava and proximal pyroclastic deposits and estimate the associated precisions. The quality of the DEMs and orthophotos, as well as the image noise due to the presence of clouds and/or volcanic plume, was considered, along with the chronology of the eruptive events (Fig. 2), when selecting which satellite datasets to use (Table 2). For example, the October 2015 dataset was excluded owing to clouds in the crater area and because no eruptive events had occurred between this dataset and the previous one (September 2015, with minor plume coverage). Prior to evaluate elevation differences (residuals) between the satellites and the 2007 data (GSDs of 1 m and 10 m, respectively), satellite DEMs were resampled to 10 m. However, pairs composed of two satellite DEMs were compared at their original GSD. A number of check areas (500 × 500 m^2) that should not have changed between subsequent datasets and that covered different slopes were defined around Etna's summit and around the 2008–2016 lava flow fields (Fig. 4a–d).

Table 1 Multi-temporal satellite datasets used to analyse the morphological evolution of Etna summit area

Date	Satellite	Acquisition mode	Spatial resolution (m)	% cloud cover	Quality/disturbs	Time interval (days)
07 August 2012	Worldview	Stereo couple	0.5	8	Volcanic plume from the craters and clouds southward of the crater area	-
12 May 2013	Pleiades-1A	Stereo couple	0.5	4	Clouds covering the Valle del Bove	275
05 September 2015	Pleiades-1A	Tristereo	0.5	2	Volcanic plume from the craters	833
07 October 2015	Pleiades-1B	Tristereo	0.5	4	Clouds coverage on the craters	32
18 December 2015	Pleiades-1A	Tristereo	0.5	0	Presence of snow in the north area	71
24 December 2015	Pleiades-1B	Tristereo	0.5	0	Widespread snow	6
18 July 2016	Pleiades-1A	Tristereo	0.5	0	Clean	204

The elevation residuals, measured inside each check area, showed Gaussian distributions for all the DEM pairs. Average residuals and standard deviations from − 1.2 to − 0.1 m and from 2.6 to 5.3 m, respectively, were obtained for pairs composed of two satellite DEMs (Fig. 4e–g and Table 3). Average residuals of 41.9–43.7 m (due to the different altimetry references) and standard deviations of 2.3–4.3 m were obtained for the pairs having the 2007 DEM as pre-event surface. To co-register DEMs in individual pairs, the average residuals have been subtracted from the elevations of each resampled Pleiades DEM, obtaining corrected residuals with average check values of around zero (Table 4). The overall quality of the datasets (2007–2016 DEMs) is summarized in Fig. 4h which shows the distributions of the elevation residuals estimated for all the check areas.

Before quantifying the new volcanic products, a further check based on an analysis of the orthophotos and shaded relief maps was applied for removing, from the selected DEMs, the values corresponding to artefacts due to volcanic plume and/or clouds in the satellite images. A natural neighbour interpolation was then performed for filling the gaps created during the artefact removal. Post-event orthophotos were analysed for manually delineating the lava fields, the base of the NSEC cone and the VOR pyroclastic proximal deposits. Delineation of the lava fields and VOR deposits was verified by checking elevation differences. The NSEC cone base was checked on post-event slopes from the resampled satellite DEMs, which highlight the abrupt slope changes at the transition from steep cone sides to the gentler sloping areas around it. The polygons of the volcanic products were then used to extract, for each DEM pair, a number of rasters representing the thickness of the different lava fields, the NSEC cone and the VOR proximal deposits. For each raster, the covered area was determined by multiplying the area of a cell by the number of pixels, while the bulk volume was measured by summing the products of cell area and interpolated thickness. The volume standard deviations (σ_V) were calculated from the variance propagation law (Coltelli et al. 2007):

$$\sigma_V = \sqrt{\sum_{ij}\left(\Delta x^4 \cdot \sigma_{\Delta z}^2 + 4 \cdot \Delta z_{ij}^2 \cdot \Delta x^2 \cdot \sigma_{\Delta x}^2\right)}$$

where $\sigma_{\Delta x}$ and $\sigma_{\Delta z}$ are the planimetric and vertical accuracies set equal to the DEM GSD and to the standard deviations of check residuals. For each lava field, we also measured the average and maximum thicknesses as well as the maximum length. For the NSEC cone, we also quantified the maximum height and maximum elevation above sea level (a.s.l.).

Since the time intervals covered by Pleiades pairs have durations of ~ 2–24 months, the analysed DEM pairs cover from one to fifteen different eruptive events, separated by pauses lasting from a few hours up to 10 months. Pairs E and F were the only ones that enabled mapping of individual effusive events producing single lava flows into the VdB (Table 2). Therefore, we generally measured cumulative volumes for both the lava fields and the proximal deposits and we divided these quantities by the corresponding cumulative durations of all the effusive/explosive events (occurring between the two analysed DEMs) to obtain multi-event eruption rates (mER) and multi-event Deposition Rates (mDR). A multi-event rate can be seen as the average value of the mean output rate (final volume divided by the total duration of an event, Harris et al. 2007) for all the single events occurring between two surveys. This quantity has the disadvantage of smoothing the differences between the various events; nevertheless, it is the only output rate that can be evaluated in a posteriori analysis of a series of past eruptions; thus, it still furnishes data useful for investigating the volcano behaviour.

Bulk volumes of lava flow fields and proximal deposits (NSEC cone and VOR) were converted to Dense Rock Equivalent (DRE) to take into account the variable vesicularity of effusive and explosive products by using average porosities of 20% and 50%, respectively (Andronico et al. 2018). It is not easy to estimate the porosity of proximal deposits inside VOR, and the actual value could be lower and closer to that of lava flows. The DRE volumes of distal tephra deposited during all paroxysmal events between each DEM pair were then estimated as 4% of the total erupted magma, on the basis of the relative percentages of lava and tephra assessed for the 25–26 October 2013 Etnean lava fountain (Andronico et al. 2018). The sum of volumes measured for lava and proximal deposits and those estimated for distal deposits gave the total DRE volume of erupted magma. The magma output rate was evaluated by dividing the volume emplaced between two surveys for the corresponding time span, while the average output rate was estimated by considering the total volume over the entire investigated time period.

Results

Geometry and rate of emplacement of the lava fields

We measured the bulk volumes and multi-event eruption rates of Etna lava fields emplaced during a series of eruptive events occurred from May 2008 to May 2016 (Table 5 and Fig. 5). Volumes of the same order of magnitude were erupted during the 2008–2009 eruption and the first thirty-eight NSEC paroxysms, lasting in total ~ 420 days and ~ 2.3 days, respectively. The following fifteen events erupted about half of that volume. Finally, single effusive events and BN overflows erupted quite low lava volumes.

Events that were mainly effusive had eruption rates ranging between ~ 2 m^3/s (2008–2009) and ~ 14 m^3/s (6–8 December 2015). Periods containing several paroxysms presented mER as high as ~ 398 m^3/s (January 2011–April 2013). When the

Table 2 Selected DEM pairs, events and style of activity covered

DEM pair	Pre-event DEM	Post-event DEM	Time interval (days)	Eruptive events from	Eruptive events between the two DEMs	Eruption style
A	August 2007	07 August 2012	~ 1769	SEC	3 paroxysms: 4–5 September 2007, 23–24 November 2007 and 10 May 2008	Explosive and effusive
				Fissure in VdB	2008/09 lateral eruption	Effusive
				NSEC	25 paroxysms between 12 January 2011 and 24-04-2012	Explosive and effusive
B	August 2007	12 May 2013	~ 2071	SEC	3 paroxysms: 4–5 September 2007, 23–24 November 2007 and 10 May 2008	Explosive and effusive
				Fissure in VdB	2008/09 lateral eruption	Effusive
				NSEC	38 paroxysms between 12 January 2011 and 28-04-2013	Explosive and effusive
C	August 2007	05 September 2015	~ 2904	SEC	3 paroxysms: 4–5 September 2007, 23–24 November 2007 and 10 May 2008	Explosive and effusive
				Fissure in VdB	2008/09 lateral eruption	Effusive
				NSEC	47 paroxysms between 12 January 2011 and 31 January 2015	Explosive and effusive
				Fissures on NSEC flanks	5 events between 14 December 2013 and 12 May 2015	Effusive
				Fissure at NEC base	1 event between 05 July 2014 and 10 August 2014	Effusive
D	12 May 2013	05 September 2015	833	NSEC	9 paroxysms between 26 October 2013 and 31 January 2015	Explosive and effusive
				Fissures on NSEC flanks	5 events between 14 December 2013 and 16 May 2015	Effusive
				Fissure at NEC base	1 event between 03 July 2014 and 10 August 2014	Effusive
E	05 September 2015	18 December 2015	103	Fissure on NSEC flanks	1 event on 06–08 December 2015	Effusive
				VOR	4 paroxysms on 03–05 December 2015	Explosive
F	18 December 2015	18 July 2016	210	Fissure at NEC base	1 event on 18–19 May 2016	Effusive
				VOR	3 paroxysms on 18–21 May 2016	Explosive
				BN	3 overflows on 18–21 May 2016	Effusive
G, H	August 2007	18 December 2015, 24 December 2015	~ 3007, ~ 3013	SEC	3 paroxysms: 4–5 September 2007, 23–24 November 2007 and 10 May 2008	Explosive and effusive
				Fissure in VdB	2008/09 lateral eruption	Effusive
				NSEC	47 paroxysms between 12 January 2011 and 31 January 2015	Explosive and effusive
				Fissure at NEC base	1 event between 05 July 2014 and 10 August 2014	Effusive
				VOR	4 paroxysms on 03–05 December 2015	Explosive
I	August 2007	18 July 2016	~ 3250	SEC	3 paroxysms: 4–5 September 2007, 23–24 November 2007 and 10 May 2008	Explosive and effusive
				Fissure in VdB	2008/09 lateral eruption	Effusive
				NSEC	47 paroxysms between 12 January 2011 and 31 January 2015	Explosive and effusive

Table 2 (continued)

DEM pair	Pre-event DEM	Post-event DEM	Time interval (days)	Eruptive events from	Eruptive events between the two DEMs	Eruption style
				Fissure at NEC base	2 events between 05 July 2014 and 10 August 2014 and on 18–19 May 2016	Effusive
				VOR	7 paroxysms: 4 on 03–05 December 2015 and 3 on 18–21 May 2016	Explosive
				BN	3 overflows on 18–21 May 2016	Effusive

lava flow fields were produced by both long-lasting effusive events and short-lasting paroxysms, the estimated mER were quite low, ~ 4 m^3/s and ~ 11 m^3/s for 15 events (October 2013–May 2015) and 53 events (January 2011–September 2015), respectively. Finally, overflows from summit craters concurrent with paroxysmal activity (May 2016) had an intermediate mER ≅ 71 m^3/s.

Distribution and rate of emplacement of the proximal deposits

The proximal pyroclastic deposits of 45 paroxysmal events, between 2011 and 2015, led to the growth of the NSEC cone to ~ 46×10^6 m^3, over a total duration of ~ 4 days (mDR ≅ 137 m^3/s). About half of the pyroclastic deposits accumulated during the first 25 paroxysms (2011–2012) over total duration of ~50 h (mDR ≅ 117 m^3/s). Thirteen more paroxysms before April 2013, over a total duration of ~ 12 h, added ~ 10×10^6 m^3 (mDR ≅ 240 m^3/s). Finally, the last seven paroxysms added ~ 15×10^6 m^3, over a total duration of ~ 31 h (mDR ≅ 129 m^3/s). After September 2015, one strombolian and effusive event at NSEC produced minor growth of the cone (~ 0.3×10^6 m^3). The cone height rapidly increased to ~ 160 m during the first 25 paroxysms, then slower growth led, in 22 more paroxysms, to a maximum height of ~ 200 m corresponding to the maximum elevation of 3287 m a.s.l. (Table 6 and Fig. 6).

Approximately 6.1 and 8.4×10^6 m^3 of pyroclastic deposits accumulated inside the VOR and BN crater depressions during the four VOR paroxysms of December 2015 and all seven VOR paroxysms, having total durations of ~ 5 h and ~ 15 h, respectively (mDR ≅ 339 m^3/s and mDR ≅ 43 m^3/s). During the May 2016 paroxysms, the lava erupted from VOR filled the crater depression, partially occupied by the December 2015 deposits, and overflowed from BN (measured bulk volume ~ 3×10^6 m^3); thus, the DRE magma volume is ~ 3.4×10^6 m^3, corresponding to a magma output rate of ~ 100 m^3/s (Table 6 and Fig. 6).

Volume of erupted magma

We measured the DRE volumes of erupted magma by considering the effusive and explosive products, both distal and proximal (Fig. 7). The values obtained are ~ 57×10^6 m^3 for the 2008–2009 effusive eruption, ~ 114×10^6 m^3 for the 38 paroxysms of January 2011–April 2013, ~ 62×10^6 m^3 for the 15 events of October 2013–May 2015, ~ 9×10^6 m^3 for the five events of May–December 2015 and ~ 6×10^6 m^3 for the four events of December 2015–May 2016. Over the full 8-year time period investigated (May 2008 to May 2016), we measured a DRE volume of erupted magma equal to $248.4 \pm 2.1 \times 10^6$ m^3 (about 76% of this volume is related to lava fields). This corresponds to a multi-event eruption rate (total volume/total duration) of 5.53 m^3/s, over ~ 520 days of total duration of the eruptions, and to an average output rate of 0.98 m^3/s, over the 8 years.

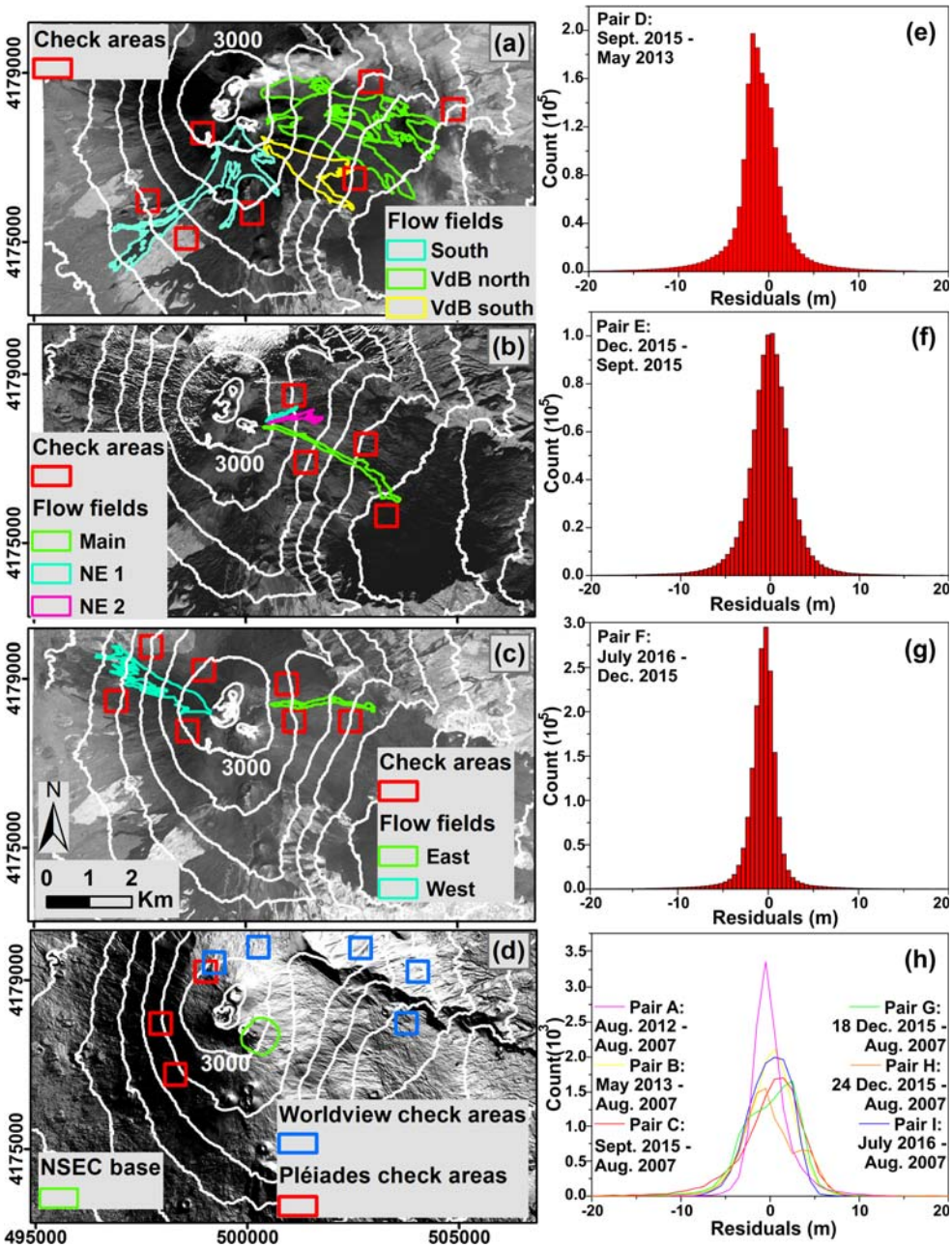

Fig. 4 **a**–**c** Flow fields and check areas shown on orthophotos from 5 September 2015, 18 December 2015 and 18 July 2016. **d** NSEC cone base and check areas shown on the 2007 shaded relief. E and N coordinates in (**a**–**c**) are the same as in (**d**); scale bars and N arrow of all maps are the same as in (**c**). Contour lines of geoid height are drawn every 250 m. **e**–**h** Distributions of the height residuals evaluated over the check areas for pairs D, E and F, as well as for each pair of Pleiades-2007 DEMs, after ellipsoid-geoid correction

Discussion

Measurements of the erupted products and of the magma output rate at active volcanoes are important both for monitoring the eruption development and quantifying the associated hazard and because they provide important data for modelling the magma dynamics driving an eruption. Current time-averaged eruption rates can be compared with past measurements giving insight into long-term trends in volcanic behaviour (e.g. Wadge 1981; Kubanek et al. 2017; Bonny et al. 2018).

The results obtained in this work can be compared with previously published volumes of lava flows and pyroclastic

Table 3 Check area statistics for Pleiades DEM pairs

DEM pair	Number of check areas	Min res (m)	Max res (m)	Aver res (m)	Stand dev (m)
D	7	−115.5	59.1	−1.2	5.3
E	4	−42.7	40.4	−0.1	2.9
F	7	−40.6	52.8	−0.5	2.6

Table 4 Check area statistics for satellite-2007 DEM pairs, last three columns: statistics after subtracting the average residual

DEM pair	Min res (m)	Max res (m)	Aver res (m)	Stand dev (m)	Min-corrected res (m)	Max-corrected res (m)	Aver-corrected res (m)
A	22.2	57.6	41.9	2.3	− 19.7	15.7	0.01
B	19.7	67.9	43.7	2.8	− 24.0	24.2	-3.4×10^{-6}
C	− 22.5	82.0	43.1	4.3	− 65.6	39.0	1.9×10^{-6}
G	8.1	71.1	42.7	3.4	− 34.5	28.5	-3.0×10^{-6}
H	26.8	67.9	43.4	3.1	− 16.6	24.5	1.2×10^{-7}
I	31.1	53.9	42.2	2.3	− 11.1	11.7	-3.5×10^{-6}

deposits and magma output rates. Our volume estimates for the 2008–2009 and 2011–2015 lava flow fields showed a minimal discrepancy of 3–4% with those obtained applying the topographic approach to DEMs (1 m GSD) extracted on 2007 and 2010 from aerial LIDAR surveys (Behncke et al. 2016) and from a subset of our data, that is the 2005 aerophotogrammetric and the 18 December 2015 Pleiades DEMs (4 m GSD, Ganci et al. 2018). However, the volume comparisons for the NSEC and the VOR pyroclastic deposits obtained, respectively, with a Pleiades dataset (Ganci et al. 2018) and a combination of DEMs from a 2010 aerial LIDAR and photogrammetric helicopter surveys performed on December 2015 (1 m GSD, Neri et al. 2017), showed a larger discrepancy of ~ 19%. The dissimilarities for the NSEC are due to a different delimitation of the volcanic products and different pre-event DEMs, which can result in including products from previous volcanic activities. The difference for VOR could be due to plume from the summit craters that resulted in elevation outliers on Pleiades DEMs. Comparing our results with previously published works based on the measurement of flow area and thickness (planimetric approach), performed for most of the eruptive episodes, shows that values from the literature are underestimated. In particular, the lava volumes accumulated in the 38 NSEC paroxysms of 2011–2013, the 15

Table 5 Quantification of effusive products covered by DEM pairs: maximum length of flow fields (L), thicknesses (T), area (A), total bulk volume and standard deviation (V and σ_v)

DEM pair	Measured products	Not measured products	Effusion duration (days)	Max L (km)	Max T (m)	Aver T (m)	A (10^6 m^2)	V (10^6 m^3)	σ_V (10^6 m^3)	ER*/ mER (m^3/s)
B	Compound lava field in VdB from the 2008–2009 effusive eruption and 10 May 2008 SEC paroxysm	Compound lava field in VdB from 38 NSEC paroxysms owing to clouds in the post-events dataset	420.0	6.4	82.4	13.15	5.4	71.6	0.9	2.0*
C–D	Compound lava field in VdB from 38 NSEC paroxysms (January 2011–April 2013)		2.3	-	-	-	-	79.8	1.6	398.4
D	Compound lava fields in VdB and on the S flank from 14 NSEC events (7 paroxysms) and 1 from NEC base (October 2013–May 2015)	1-km-long simple flow to the NE of NSEC owing to plume in the post-eruption orthophoto	125.8	4.5	44.0	6.9	6.8	46.4	1.6	4.3
	South lava field in VdB estimated through the planimetric approach owing to clouds in the pre-event dataset									
C	Compound lava field in VdB from 52 NSEC events (47 paroxysms) and 1 from NEC base (January 2011–May 2015)		128.1	4.5	99.9	15.4	8.1	126.1	1.2	11.4
E	3 simple flows in VdB from 1 event from NSEC flank (6–8 December 2015)		2.0	3.8	24.7	4.6	0.5	2.432	0.009	14.1*
F	Simple flow in VdB from 1 event at NEC base (18–21 May 2016)		0.4	2.5	23.3	1.7	0.2	0.376	0.002	10.4*
	Compound field on the W flank from 3 events from BN (18–21 May 2016)		0.5	3.1	18.5	3.1	0.9	2.809	0.008	70.7

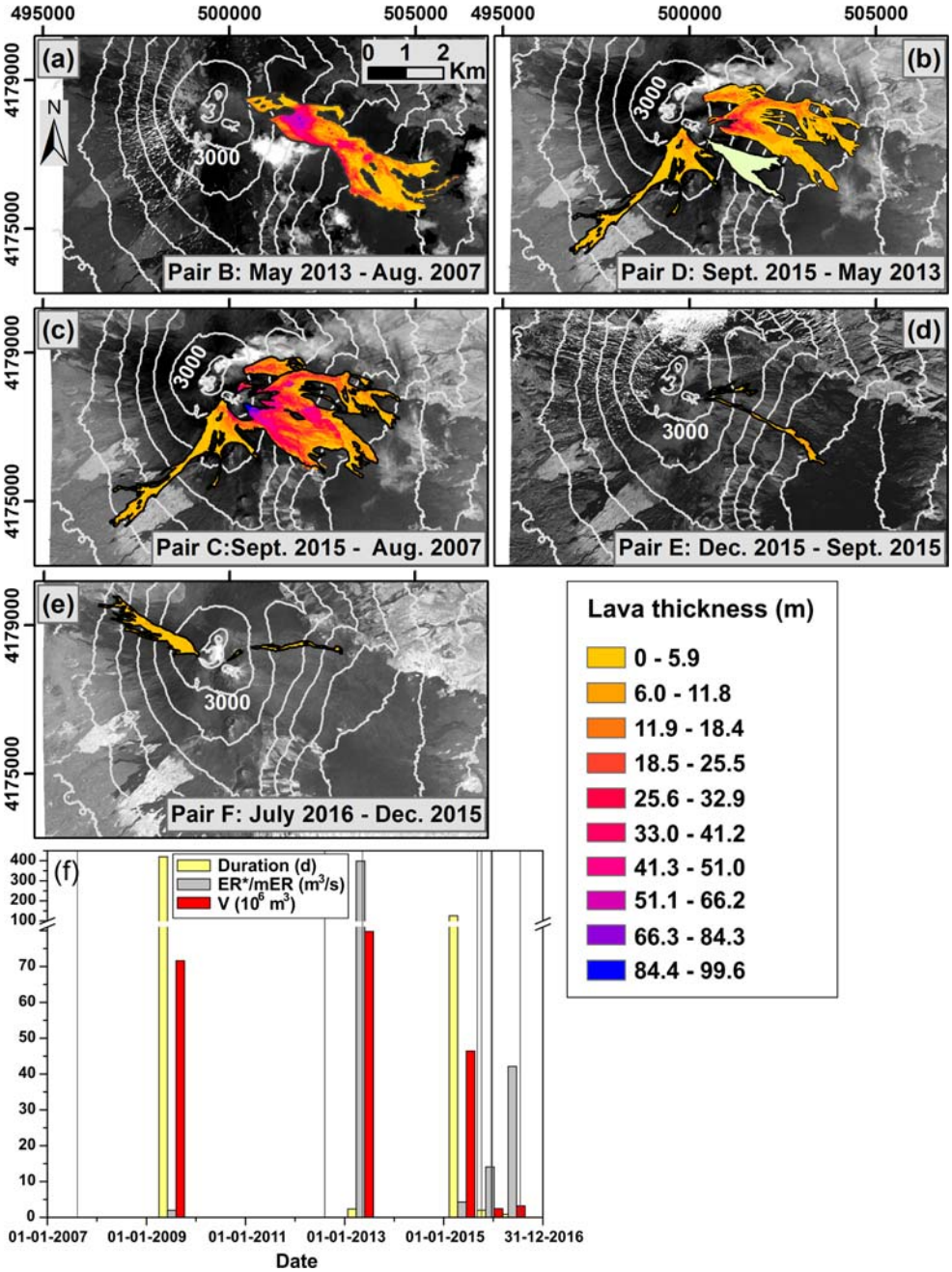

Fig. 5 (a–e) Thicknesses of the lava flow fields, shown over post-event orthophotos with contour lines of geoid height every 250 m, measured from pairs B, D, C, E and F; coordinate ranges, scale bar and north arrow in (a), as well as thickness scale are the same for all maps. (f) Total volume (V), duration and eruption/multi-event eruption rates (ER*/mER), drawn at the last event in each time interval. Grey vertical lines indicate the timing of DEM acquisitions

Table 6 Quantification of NSEC and VOR proximal deposits: area (A), maximum height and elevation (H and Elev), bulk volume and standard deviation (V and σ_V)

DEM pair	Analysed crater	Date of last event	Cumulative number of paroxysms	Cumulated fountain duration (days)	A (10^6 m^2)	Max H (m)	Max Elev (m a.s.l.)	Cumulative V (10^6 m^3)	σ_V (10^6 m^3)	mDR (m^3/s)
A	NSEC	23 April 2012	25	2.1	0.4	162	3225	21.2	0.9	117
B	NSEC	28 April 2013	38	2.6	0.5	174	3275	31.4	1.1	240
C	NSEC	16 May 2015	47	3.1	0.6	183	3287	45.9	1.4	129
H	NSEC	08 December 2015	47	3.1	0.6	198	3287	46.2	1.4	0
E, H	VOR	05 December 2015	4	0.2	0.5	-	-	6.07	0.03	336
I	VOR	21 May 2016	7	0.6	0.3	-	-	8.35	0.03	448

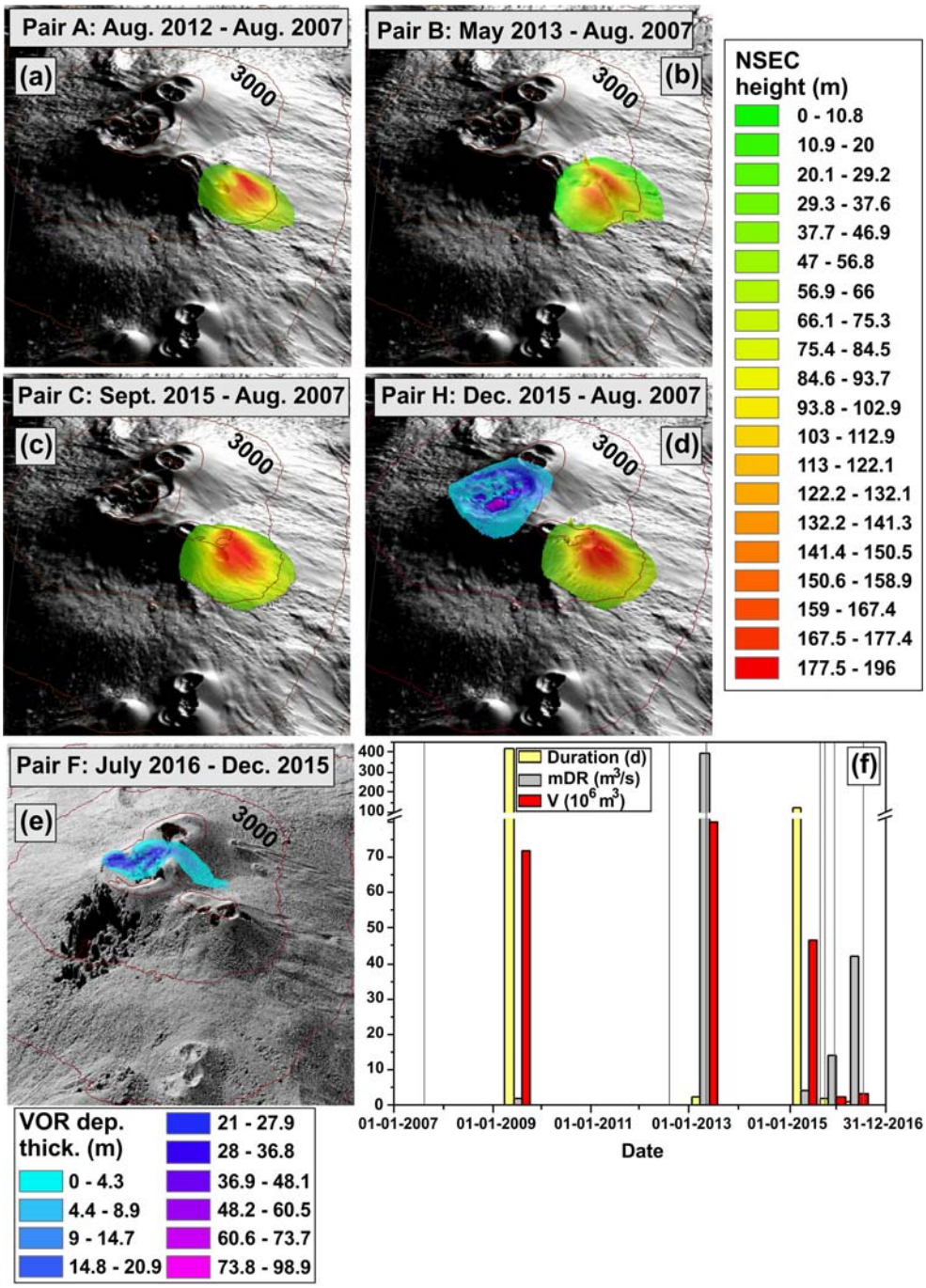

Fig. 6 (a–d) NSEC cone height measured, with respect to the 2007 DEM (background image), on August 2012, May 2013, September and December 2015 DEMs. (d–e) Thickness of VOR deposits in December 2015 and between December 2015 and July 2016. Legends are the same for all maps. Background image in (e) is 2016 shaded relief. Contour lines of geoid height are drawn every 250 m. (f) Duration, volume (*V*) and multi-event deposition rate (mDR), drawn at the last event in each time interval, for all paroxysms between each DEM pair. Grey vertical lines indicate the timing of DEM acquisitions

events of 2013–2015, the 53 events of January 2011–May 2015 and the 6–8 December 2015 effusive event are underestimated by ~47%, ~15%, ~35% and ~6%, respectively (Behncke et al. 2014; De Beni et al. 2015; Corsaro et al. 2017). The higher discrepancies obtained when considering more events derive from the error propagation during the summation of multiple volumes. Moreover, for compound lava fields formed during frequently repeated eruptive events, higher discrepancies are due to the difficulty of estimating the mean lava thickness for an irregular morphology. Therefore, the planimetric approach can be applied for rapid preliminary quantification of the area and volume of simple lava flows. However, DEMs and orthophotos from high-spatial resolution satellite stereo-pairs can effectively support the topographic approach which is more reliable when dealing with compound lava flows and wide morphological variations, such as the growth of a new pyroclastic cone.

Our results can be compared with the average values of previously published lava volumes, evaluated from thermal satellite data. These volumes are always given as ranges

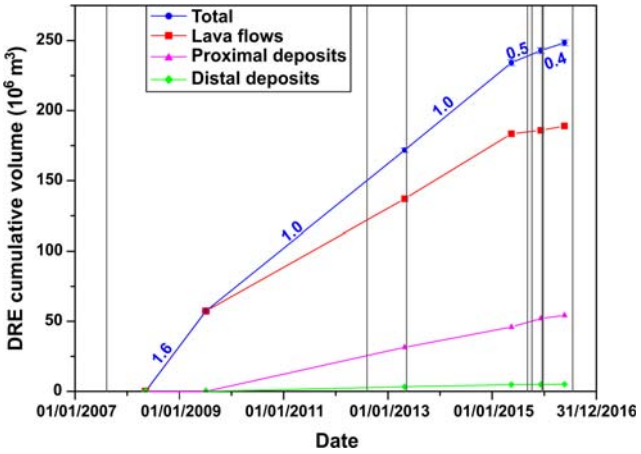

Fig. 7 Cumulative DRE volumes (drawn at the last event in each time interval) of the different volcanic products. Grey vertical lines indicate the timing of DEM acquisitions. Blue numbers are magma output rate (m^3/s) between two volume measurements

owing to the large and unavoidable uncertainty of the underlying assumptions used for converting the measured radiance to time-averaged discharge rates (TADR, Harris et al. 2007). The TADR estimates can also be influenced by the presence of an ash column that attenuates or obscures the thermal anomaly (Ganci et al. 2012). Our measurements, compared with the corresponding average volumes from thermal data, are higher by ~ 35% (Ganci et al. 2012) and ~ 5% (Harris et al. 2011) for the 2008–2009 eruption; and by ~ 16% for the 2011–2015 lava fields (Ganci et al. 2018). Our measurements correspond approximately to the upper limit of the variability range of volumes from thermal data.

By analysing the overall results, we measured a total DRE volume of ~ 248×10^6 m^3 (~ 190×10^6 m^3 from lava fields), which corresponds to a multi-event eruption rate of 5.53 m^3/s for 520 days of eruptive activity and to an average output rate of ~ 0.98 m^3/s over 8 years. Over 10 years, this would result in a total DRE volume of ~ 310×10^6 m^3. These values are in accordance with the erupted lava volumes of ~ 300×10^6 m^3 and mean output rate of 0.6–0.9 m^3/s obtained, on a decadal scale, analysing Etna's 1980–2010 effusive activity from thermal satellite data and with the 2001–2010 mean output rate of 0.97–1.07 m^3/s obtained by including tephra volumes from the literature (Harris et al. 2011). Our average output rate is ~ 20% higher than the value expected for the 1993–2013 Etna activity, analysed by combining volumes from the literature measured with different techniques, including analysis of satellite thermal data and the planimetric approach applied to the thirty-eight 2011–2013 fountains (Bonaccorso and Calvari 2013).

By analysing the output rates we measured over the different time intervals, we observed that a greater magma output (~ 1.6 m^3/s) is associated with long-lasting lateral effusive eruptions (2008–2009). An output rate of ~ 1 m^3/s was measured for the subsequent two periods (up to May 2013 and May 2013–May 2015) mostly characterized by short-lasting paroxysms interspersed with pauses lasting from a few hours to ~ 10 months. Finally, a lower output rate (~ 0.4–0.5 m^3/s) was found during two time periods (May–December 2015 and December 2015–May 2016) characterized by brief effusive events and very short paroxysms separated by pauses of a few months. Even though the eruption rate associated with each paroxysm is quite high (some hundreds of m^3/s), it appears to be insufficient to discharge all the accumulated magma and a series of repeated events can occur in very short time.

Conclusions

This work quantified the lava and the pyroclastic (proximal and distal) products erupted at Etna over an 8-year period (2008–2016), characterized by simultaneous intense explosive and effusive activity, and evaluated the corresponding magma average output rate, thus yielding data useful for analysing the long-term Etna discharge rate. Although previous research exists which quantifies Etna's recent eruptive activity using different techniques, we applied one methodology to a homogeneous and comprehensive dataset to quantify the DRE magma volumes and the output rate. In particular, we quantified the lava and proximal products, and associated uncertainties, applying the topographic approach to a time-series of co-registered DEMs and orthophotos (with 1- and 0.5-m-pixel resolutions respectively), extracted from six specifically tasked Pleiades tri-stereo pairs (with time intervals of ~ 2–24 months) plus one aerophotogrammetric DEM (10-m pixel resolution), used as reference topographic surface. Maximum percentage errors of ~ 3.4 and ~ 4.2% were obtained for the volumes of the lava fields and the NSEC cone, respectively. We then estimated the distal products by applying the percentages of lava and tephra erupted at the same time, which have been accurately quantified for the 25–26 October 2013 lava fountain of Etna in a previous research.

The performed analysis showed that specifically tasked optical images, acquired from meter-resolution satellite systems capable of daily revisits to any point on the globe, are key data for monitoring an active volcano. Such data enable a swift response to an eruptive crisis allowing a rapid, complete and accurate quantification of the volcanic products and of the related hazard, as well as the updating of topographic data. Above all, such data allow monitoring of the volcanic activity to be carried out without putting personnel at risk. Therefore, if it were possible to task Pleiades acquisitions to systematically monitor long-lasting eruptions, the collected data could be used to improve inventories of magma output rate thus contributing to both hazard assessment analysis and the understanding of system dynamics (c.f. Wadge 1981).

Our study was here successfully applied to a well-monitored volcano: Etna. The Pleiades global coverage and the theoretical possibility of daily tasking data acquisition, on user-specified areas, enable this methodology to be applied to the

monitoring of remote or hazardous volcanoes that may be difficult to access for repeat field surveys.

Acknowledgements We acknowledge Pierre Briole and Marcello de Michele for providing Pleiades data, analysed in this work, through the Space Volcano Observatory sur Pleiades (SVOP) project (http://volcano.iterre.fr/svo_projects). We are grateful to Massimo Fabris for processing the Worldview 2012 data to extract the DEM of the NSEC cone. We are grateful to Eisuke Fujita, an anonymous reviewer and the associate editor, Michael R. James, for their comments and feedback which greatly improved this manuscript and to William Moreland for improving the English.

References

Andronico D, Behncke B, De Beni E, Cristaldi A, Scollo S, Lopez M, Lo Castro MD (2018) Magma budget from lava and tephra volumes erupted during the 25-26 October 2013 lava fountain at Mt Etna. Front Earth Sci 6:116. https://doi.org/10.3389/feart.2018.00116

Baldi P, Fabris M, Marsella M, Monticelli R (2005) Monitoring the morphological evolution of the Sciara del Fuoco during the 2002–2003 Stromboli eruption using multi-temporal photogrammetry. ISPRS J Photogramm Remote Sens 59:199–211

Bagnardi M, González PJ, Hooper A (2016) High-resolution digital elevation model from tri-stereo Pleiades satellite imagery for lava flow volume estimates at Fogo Volcano. Geophys Res Lett 43:6267–6275. https://doi.org/10.1002/2016GL069457

Behncke B, Branca S, Corsaro RA, De Beni E, Miraglia L, Proietti C (2014) The 2011–2012 summit activity of Mount Etna: birth, growth and products of the new SE crater. J Volcanol Geotherm Res 270:10–21. https://doi.org/10.1016/j.jvolgeores.2013.11.012

Behncke B, Fornaciai A, Neri M, Favalli M, Ganci G, Mazzarini F (2016) Lidar surveys reveal eruptive volumes and rates at Etna, 2007–2010. Geophys Res Lett 43:4270–4278. https://doi.org/10.1002/2016GL068495

Boissin MB, Gleyzes A, Tinel C (2012) The Pleiades system and data distribution. In: IEEE International Geoscience and Remote Sensing Symposium, Munich, Germany, pp 7098–7101

Bonaccorso A, Calvari S (2013) Major effusive eruptions and recent lava fountains: balance between expected and erupted magma volumes at Etna volcano. Geophys Res Lett 40:6069–6073. https://doi.org/10.1002/2013GL058291

Bonny E, Thordarson T, Wright R, Höskuldsson A, Jónsdóttir I (2018) The volume of lava erupted during the 2014 to 2015 eruption at Holuhraun, Iceland: a comparison between satellite- and ground-based measurements. J Geophys Res Solid Earth 123:5412–5426. https://doi.org/10.1029/2017JB015008

Calvari S, Coltelli M, Neri M, Pompilio M, Scrivano V (1994) The 1991-1993 Etna eruption: chronology and lava flow-field evolution. Acta Volcanol 4:1–14

Coltelli M, Proietti C, Branca S, Marsella M, Andronico D, Lodato L (2007) Analysis of the 2001 lava flow eruption of Mt. Etna from three-dimensional mapping. J Geophys Res 112:F02029. https://doi.org/10.1029/2006JF000598

Coltelli M, D'Aranno PJV, De Bonis R, Guerrero F, Marsella M, Nardinocchi C, Pecora E, Proietti C, Scifoni S, Scutti M, Wahbeh W (2017) The use of surveillance cameras for the rapid mapping of lava flow: an application to Mount Etna Volcano. Remote Sens 9:192. https://doi.org/10.3390/rs9030192

Corsaro RA, Andronico D, Behncke B, Branca S, De Beni E, Caltabiano T, Ciancitto F, Cristaldi A, De Beni E, La Spina A, Lodato L, Miraglia L, Neri M, Salerno G, Scollo S, Spata G (2017) Monitoring the December 2015 summit eruptions of Mt. Etna (Italy): implications on eruptive dynamics. J Volcanol Geotherm Res 341:53–69. https://doi.org/10.1016/j.jvolgeores.2017.04.018

De Beni E, Behncke B, Branca S, Nicolosi I, Carluccio R, D'Ajello Caracciolo F, Chiappini M (2015) The continuing story of Etna's New Southeast Crater (2012–2014): evolution and volume calculations based on field surveys and aerophotogrammetry. J Volcanol Geotherm Res 303:175–186. https://doi.org/10.1016/j.jvolgeores.2015.07.021

Dvigalo V, Shevchenko A, Svirid I (2016) Photogrammetric survey in volcanology: a case study for Kamchatka active volcanoes. In: Nemeth K (ed) Updates in volcanology - from volcano modelling to volcano geology. InTech, pp 55–79. https://doi.org/10.5772/63577

Eisank C, Rieg L, Klug C, Kleindienst H (2015) Semi-global matching of Pleiades tri-stereo imagery to generate detailed digital topography for high-alpine regions. GI_Forum – J Geogr Inf Sc 3:168–177. https://doi.org/10.1553/giscience2015s168

Francis P, Rothery D (2000) Remote sensing of active volcanoes. Annu Rev Earth Planet Sci 28:81–106

Fraser CS, Dial G, Grodecki J (2006) Sensor orientation via RPCs. ISPRS J Photogramm Remote Sens 60(3):182–194

Ganci G, Vicari A, Cappello A, Del Negro C (2012) An emergent strategy for volcano hazard assessment: from thermal satellite monitoring to lava flow modelling. Remote Sens Environ 119:197–207

Ganci G, Cappello A, Bilotta G, Herault A, Zago V, Del Negro C (2018) Mapping volcanic deposits of the 2011–2015 Etna eruptive events using satellite remote sensing. Front Earth Sci 6:83. https://doi.org/10.3389/feart.2018.00083

Gwinner K, Coltelli M, Flohrer J, Jaumann R, Matz KD, Marsella M, Roatsch T, Scholten F, Trauthan F (2006) The HRSC-AX Mt. Etna project: high-resolution orthoimages and 1 m DEM at regional scale. In: Proceedings ISPRS Archives 23, 1, From Sensors to Imagery (Paris, 4–6 July 2006), 6 pp, T05–23

Harris AJL, Dehn J, Calvari S (2007) Lava effusion rate definition and measurement: a review. Bull Volcanol 70:1–22. https://doi.org/10.1007/s00445-007-0120-y

Harris AJL, Steffke A, Calvari S, Spampinato L (2011) Thirty years of satellite-derived lava discharge rates at Etna: implications for steady volumetric output. J Geophys Res 116:B08204. https://doi.org/10.1029/2011JB008237

Honda K, Nagai M (2002) Real-time volcano activity mapping using ground-based digital imagery. ISPRS J Photogramm Remote Sens 57:159–168

http://volcano.iterre.fr/svo_projects. Accessed 18 March 2019

Kubanek J, Westerhaus M, Heck B (2017) TanDEM-X time series analysis reveals lava flow volume and effusion rates of the 2012–2013 Tolbachik, Kamchatka fissure eruption. J Geophys Res Solid Earth 122:7754–7774. https://doi.org/10.1002/2017JB014309

Marsella M, Proietti C, Sonnessa A, Coltelli M, Tommasi P, Bernardo E (2009) The evolution of the Sciara del Fuoco subaerial slope during the 2007 Stromboli eruption: relation between deformation processes and effusive activity. J Volcanol Geotherm Res 182:201–213

Marsella M, Nardinocchi C, Proietti C, Daga L, Coltelli M (2014) Monitoring active volcanos using aerial images and the orthoview tool. Remote Sens 6:12166–12186. https://doi.org/10.3390/rs61212166

Martino M, Marsella M, Scifoni S Coltelli M, Proietti C, Chowdhury TA, Minet C, Giannone F (2016) Monitoring an active volcanic area and mapping lava flows with multisource data: the case of Mount Etna from 2011 to 2015. EEEIC 2016 - International Conference on Environment and Electrical Engineering, 7–10 June 2016. https://doi.org/10.1109/EEEIC.2016.7555732

Mouginis-Mark PJ, Pieri DC, Francis PW, Wilson L, Self S, Rose WI, Wood CA (1989) Remote sensing of volcanos and volcanic terrains. EOS Trans Am Geophys Union 70:1567–1575. https://doi.org/10.1029/89EO00396

Naranjo MF, Ebmeier SK, Vallejo S, Ramón P, Mothes P, Biggs J, Herrera F (2016) Mapping and measuring lava volumes from 2002 to 2009 at El Reventador Volcano, Ecuador, from field measurements and satellite remote sensing. J Appl Volcanol 5:8. https://doi.org/10.1186/s13617-0160048-z

Neri M, De Maio M, Crepaldi S, Suozzi E, Lavy M, Marchionatti F, Calvari S, Buongiorno MF (2017) Topographic maps of Mount Etna's summit craters, updated to December 2015. J Maps 13(2): 674–683. https://doi.org/10.1080/17445647.2017.1352041

Rowland S, Harris A, Wooster M, Amelung F, Garbeil H, Wilson L, Mouginis-Mark P (2003) Volumetric characteristics of lava flows from interferometric radar and multispectral satellite data: the 1995 Fernandina and 1998 Cerro Azul eruptions in the western Galapagos. Bull Volcanol 65:311–330. https://doi.org/10.1007/s00445-002-0262-x

Stevens NF, Wadge G, Murray JB (1999) Lava flow volume and morphology from digitised contour maps: a case study at Mount Etna, Sicily. Geomorphology 28:251–261

Wadge G (1981) The variation of magma discharge during basaltic eruptions. J Volcanol Geotherm Res 11:139–168

www.pcigeomatics.com. Accessed 18 March 2019